A Comparative Evaluation for Differentially Private Image Obfuscation

Dominick Reilly
Department of Computer Science
UNC Charlotte
dreilly1@uncc.edu

Liyue Fan
Department of Computer Science
UNC Charlotte
liyue.fan@uncc.edu

***Abstract*—As a substantial amount of image data is continuously being collected, ensuring the privacy of image data is a significant concern. Image data may contain sensitive information, such as face and iris, which can be misused if in the hands of an adversary. Widely used image obfuscation methods include blurring or mosaicing those sensitive regions. However, they are prone to inference attacks, and do not provide quantifiable privacy guarantees. Recently, several image/video obfuscation approaches have been proposed that satisfy the rigorous notion of differential privacy. In this work, we synthesize those approaches in the context of obfuscating face and iris images and analyze their privacy guarantees. Furthermore, we conduct a comparative evaluation of those methods regarding practical utility and privacy protection, with real-world face and iris image datasets. We find that DP-SVD performs best on several privacy and utility measures while providing provable privacy guarantees. Moreover, we recommend practices for applying differentially private image obfuscation to novel data requiring unique privacy and utility constraints.**

I. Introduction

An immense amount of image data is captured everyday from a variety of sensors, and has proven to be an invaluable asset for researchers, allowing for advancements in intelligent traffic monitoring [15] and early screening of mental illnesses [20]. The wide-scale release of such data would be of great benefit to society; however, without proper precautions, individual's privacy will be put at risk. For instance, images from traffic cameras may expose a wide array of information, such as faces, license plate numbers, and locations, which may be used by adversaries track an individual. Eye tracking images captured by virtual reality headsets may expose a user's iris signature, allowing an impostor to compromise data secured by iris authentication. In order to protect user privacy, these images must be obfuscated before sharing with the un-trusted parties.

Standard approaches to obfuscating images consist of methods such as pixelization [17] and blurring [23]. Though these approaches may visually appear to hide sensitive information, studies have shown that deep convolutional neural networks (CNNs) are effective at re-identifying images obfuscated with these approaches [11], [17]. More complex obfuscation approaches exist that utilize generative adversarial networks (GANs) to in-paint sensitive image regions [21], [25]; however, these methods require large amounts of training data that may not be readily available. Furthermore, these obfuscation approaches do not allow the privacy to be effectively bounded, i.e. they do not allow the quantification of sensitive information that may be leaked in the obfuscated image.

In order to address these challenges, novel image obfuscation techniques providing rigorous privacy protections must be developed. Differential privacy [4] is the state-of-the-art notion for quantifying privacy leakage in sensitive databases and has been adopted in large-scale by organizations such as Google [9], Apple [26], and the Census Bureau [14]. An obfuscation mechanism satisfying differential privacy provides a guarantee that the output of any two neighboring databases differing by one entry will be indistinguishable to an adversary, regardless of any background knowledge the adversary may have.

Though widely adopted as a means of obfuscating databases, few studies have adopted the notion of differential privacy to image/video obfuscation. Current differentially private image obfuscation methods such as [6], [7] are able to provide ϵ-differential privacy, while [13] provides (ϵ, δ)-differential privacy. Additionally, [27] provides differentially privacy video analysis; in our work, we adapt the proposed method to provide differential privacy protection to image data.

In this study, we propose a comparative evaluation of the current differentially private image obfuscation methods. Our specific contributions are: (1) we provide a review of existing DP algorithms for image obfuscation and highlight the technical steps with consistent notation; (2) we conduct a comparative evaluation using real eye and face datasets and widely adopted utility measures, such as MSE and SSIM; (3) we further evaluate existing methods regarding their usefulness for specific applications, e.g., eye-tracking, and the practical privacy protection, e.g., empirical risk measures; (4) last but not least, we discuss the results thoroughly and provide recommendations to domain applications with different privacy/utility preferences.

A. Differential Privacy Preliminaries

Differential privacy is the state-of-the-art notion for quantifying privacy leakage in statistical databases containing sensitive data. The objective of differential privacy is to guarantee that any individual contained in a database will not carry privacy risk, regardless of external information that is available or may become available in the future.

Given two neighboring databases, $\mathcal{D}$ and $\mathcal{D}'$, that differ by at most one element, a randomized mechanism $\mathcal{M}$ satisfies (ϵ, δ)-differential privacy [5] if for any $\mathcal{Z} \in range(\mathcal{M})$,

$$\Pr[\mathcal{M}(D) = \mathcal{Z}] \leq e^{\epsilon} \cdot \Pr[\mathcal{M}(D') = \mathcal{Z}] + \delta. \quad (1)$$

The ϵ and δ parameters specify the degree of privacy provided by the mechanism, also known as the privacy budget. Here, $\epsilon > 0$ bounds the difference between output probabilities of two neighboring databases $D, D^{'}$. In addition, $\delta \in [0, 1]$ accounts for the probability of *bad events* that might lead to a privacy breach. Typically, smaller ϵ and δ values indicate stronger privacy protection, and vice versa.

An advantage of DP is its resistance to post-processing [5], i.e., any computation performed on the output of a DP mechanism would not incur additional privacy cost. Other benefits of DP include the lightweight computation and ease of control over the information leakage with the help of ϵ, δ parameters. Naturally, there exists a trade-off between preserving privacy and maintaining data utility.

Algorithm 1: DP-Pix

Input : Input image $\mathcal{I}$, Privacy budget ϵ, Block size b, Number of pixels m
Output: Obfuscated image satisfying ϵ-DP

blocks $\leftarrow$ partition $\mathcal{I}$ into blocks of size $b \times b$
foreach block *in* blocks **do**
  average $\leftarrow$ average pixel intensity of block
  noise $\leftarrow$ noise drawn from $Laplace(0, \frac{255m}{b^2\epsilon})$
  assign intensity of pixels in block to average + noise
end
$\hat{\mathcal{I}} \leftarrow$ output image constructed from blocks

II. Obfuscation Methods

A. DP-Pix

Differentially private pixelization [6] (DP-Pix) is the first method that provides differential privacy guarantees for publishing individual images. Given the large number of pixels contained in a typical image, directly perturbing each pixel in the source image would lead to low utility. To balance privacy and utility, DP-Pix adopts pixelization and the Laplace mechanism to satisfy differential privacy.

1) m-neighborhood: The work [6] proposes a m-neighborhood notion to define neighboring images in the context of differential privacy. Two images, I_1 and I_2, are considered neighboring if they differ by at most m pixels. By varying the value of m, the data owner can control the privacy protection offered by DP-Pix: higher m values indicate indistinguishability in a larger neighborhood, thus stronger privacy protection.

2) Private Pixelization: DP-Pix leverages pixelization to reduce the amount of noise required for differential privacy. Pixelization, *a.k.a.* mosaicing, decomposes an image into blocks by superimposing a grid on the source image, where each grid cell (i.e., super-pixel) contains $b \times b$ pixels. The value of each super-pixel is determined by averaging all pixels contained in the grid cell. To achieve ϵ-DP, a perturbation noise is sampled from a Laplacian distribution with mean 0 and scale $\frac{255m}{b^2\epsilon}$ and added to each grid cell. Algorithm 1 depicts the steps taken by DP-Pix.

B. DP-Samp

A recent work [27] proposed a pixel-sampling method to protect the presence of visual elements (e.g., persons and objects) in videos. In this study, we adapt the video sanitization method [27] to protecting up to m pixels in a source image and name the new method as DP-Samp. DP-Samp consists of four steps, namely pixel clustering, budget allocation, pixel sampling, and interpolation.

1) Pixel Clustering: The goal of clustering is to select pixel intensities that are useful for reconstructing the image. An intuitive approach is to select the most frequent intensities in the image; however, this approach may not capture the structures of images containing large regions with slightly varying intensities. The video-based method [27] adopted multi-scale analysis [29] to partition each visual element in k cells; as such methods do not apply to a single image, we propose to generate k pixel clusters with K-means[1], in order to capture diverse regions in the image. The most frequent intensity in each cluster, $\Psi_{1:k}$, will be candidates for pixel sampling. Note that the clustering step is conducted in the *public* setting, same as the multi-scale analysis step in [27]. The integration with differentially private clustering methods, such as [24], is out of the scope of this work.

In Figure 2, we present the clustering results on eye and face images at varying values of k. Pixels chosen as sampling candidates are highlighted in green. From the images, we see that a higher number of clusters may provide a better coverage of important structures in both datasets, possibly allowing an more effective reconstruction of the image from sampled pixels.

2) Budget Allocation: The privacy budget ϵ must be split amongst all selected intensities in Ψ so that the budget is completely utilized. Similar to [27], DP-Samp allocates higher privacy budgets to intensities occurring more frequently. Let $\text{Freq}(\Psi_i)$ be the number of pixels in the source image with intensity Ψ_i, then the privacy budget of the ith intensity can be computed as:

$$\epsilon(\Psi_i) = \frac{\epsilon \cdot \text{Freq}(\Psi_i)}{\sum_{j=1}^{k}(\text{Freq}(\Psi_j))} \quad (2)$$

3) Pixel Sampling: From each intensity Ψ_i, we randomly sample x_i pixels from the source image, which preserve their location and intensity. It has been shown in [27] that selecting x_i as follows satisfies ϵ-DP. The value of x_i is dependent on the budget allocated to the intensity:

$$\max x_i, s.t. \binom{c_i}{x_i} \Big/ \binom{c_i - m}{x_i} \leq e^{\epsilon(\Psi_i)}, \quad (3)$$

[1] other clustering methods, such as hierarchical clustering, are also applicable.

Algorithm 2: DP-Samp

Input : Input image $\mathcal{I}$, Privacy budget ϵ, Number of clusters k, Number of pixels m
Output: Obfuscated image satisfying ϵ-DP

perform pixel clustering to generate k clusters
calculate most frequent intensity in each cluster $(\Psi_1, ..., \Psi_k)$
// Budget allocation
foreach $\Psi_i, i \in [1, k]$ **do**
  compute the privacy budget $\epsilon(\Psi_i)$ with Eq. 2
end
// Pixel sampling
foreach $\Psi_i, i \in [1, k]$ **do**
  compute maximum x_i with Eq. 3
  randomly select x_i pixels from $\mathcal{I}$ with intensity Ψ_i to preserve in output image $\hat{\mathcal{I}}$
end
// Interpolation
linear interpolate non-sampled pixels in $\hat{\mathcal{I}}$

(a) Input Image (b) Sampled Pixels (c) Interpolated Image

Fig. 1: Sampled and interpolated images generated by DP-Samp with $\epsilon = 3$, $k = 15$, $m = 1$

where c_i is the count of pixels with intensity Ψ_i in the image, m is the number of pixels that are allowed to differ between neighboring images, and $\epsilon(\Psi_i)$ is the privacy budget allocated to Ψ_i according to Equation 2.

4) Interpolation: Similar to [27], DP-Samp performs linear interpolation on the sampled pixels to estimate the values of those non-sampled pixels. Utilizing the post-processing property of DP [5], the interpolation does not inflict additional privacy loss in the output image $\hat{\mathcal{I}}$. The sampled pixels and the final interpolated image are shown in Figure 1, we see that pixel interpolation produces an accurate estimation of the input, despite sparsely sampled pixels.

C. DP-SVD

Differentially private singular value decomposition [7] (DP-SVD) adopted to singular value decomposition to decompose a source image into constituent feature matrices that capture perceptual and geometric features in the image. Furthermore, the work developed a novel sampling mechanism in high-dimensional space which achieves metric-based privacy [2]. The singular values are considered as sensitive information as they represent the magnitudes of the geometric features.

1) Singular value decomposition: The SVD decomposition is in the form $I = U\Sigma V^T$, where I is the source image, U and V consist of singular vector matrices that capture geometric features, and Σ consists of the singular value matrix that capture the magnitudes of features in U and V. It can be been shown that these constituent feature matrices capture perceptual and geometric features that are able to reconstruct images perceptually indistinguishable from the source image.

2) Metric privacy: The intuition of DP-SVD is to provide indistinguishability guarantees to visually *similar* images, similar to the geo-indistinguishability [1] for location data. To that end, metric-based privacy [2], i.e., $\epsilon \cdot d_{\mathcal{X}}$-privacy, was adopted in [7] for protecting image data. Metric privacy extends differential privacy to a set of secrets $\mathcal{X}$ that are equipped with a distance metric, i.e., $d_{\mathcal{X}}$, and guarantees a level of indistinguishably that is proportional to the distance between secrets. Specifically:

Definition 1. [2] A mechanism $K : \mathcal{X} \to \mathcal{P}(\mathcal{Z})$ satisfies $\epsilon \cdot d_{\mathcal{X}}$-privacy, *iff* $\forall x, x' \in \mathcal{X} : d_{\mathcal{P}}(K(x), K(x')) \leq d_{\mathcal{X}}(x, x')$, or equivalently:

$$K(x)(Z) \leq e^{\epsilon \cdot d_{\mathcal{X}}(x,x')} K(x')(Z) \quad \forall Z \in \mathcal{F}_{\mathcal{Z}} \tag{4}$$

where $\mathcal{Z}$ is the output space of K, $\mathcal{F}_{\mathcal{Z}}$ is a σ-algebra over $\mathcal{Z}$, and $\mathcal{P}(\mathcal{Z})$ is the set of probability measures over $\mathcal{Z}$.

Algorithm 3: DP-SVD

Input : Input image $\mathcal{I}$, Privacy budget ϵ, Number of eigenvalues i
Output: Obfuscated image satisfying $\epsilon \cdot d_i$-privacy

decompose $\mathcal{I}$ using SVD: U, Σ, V^T
$\hat{\Sigma} \leftarrow i$ largest singular values of Σ. $(\hat{\Sigma}_1, ..., \hat{\Sigma}_i)$
$\mathcal{N} \leftarrow$ noise vector sampled according to Eq. 5
for $j \in [1, i]$ **do**
  $\hat{\Sigma}_j \leftarrow \hat{\Sigma}_j + \mathcal{N}_j$
end
pad $\hat{\Sigma}$ with 0s for the discarded singular values
$\hat{\mathcal{I}} = U \cdot \hat{\Sigma} \cdot V$

3) Private Sampling: DP-SVD [7] achieves metric privacy by perturbing the first i singular values using a novel sampling method. Other singular values are discarded, and the output image is reconstructed with the privacy-enhanced singular values. Increasing i may lead to a better approximation of the input image, while inflicting a higher perturbation to achieve privacy.

Specifically, DP-SVD perturbs the first i singular values according a specific probability distribution. In an i-dimensional space, let x_0 denote the input vector, i.e., containing the real singular values. A mechanism that samples the output vector x according to following probability distributions satisfies $\epsilon \cdot d_i$-privacy [7]:

$$D_{\epsilon,i}(x_0)(x) = C_{\epsilon,i} e^{-\epsilon \cdot d_i(x_0, x)} \tag{5}$$

where d_i represents i-dimensional Euclidean distance and

$$C_{\epsilon,i} = \frac{1}{2}\left(\frac{\epsilon}{\sqrt{\pi}}\right)^i \frac{\left(\frac{i}{2} - 1\right)!}{(i-1)!} \tag{6}$$

i is assumed even without loss of generality. Details of sampling according to Equation 5 are described in [7].

D. Snow

The intuition of Snow [13] is the introduction of noise to an image via randomly re-assigning pixel intensities to a constant

Dataset	DP-Pix (b)	DP-Samp (k)	DP-SVD (i)
CASIA	6	28	6
AT&T	4	48	4

Table I: Default algorithm parameters used in experiments

value. The parameter p controls the proportion of pixels that will be re-assigned and is related to the privacy parameter δ. It is shown in [13] that the method achieves $(0, \delta)$-differential privacy with $\delta = 1 - p$.

Algorithm 4: Snow

Input : Input image $\mathcal{I}$, Privacy budget δ
Output: Obfuscated image satisfying $(0, \delta)$-DP

$\mathsf{p} \leftarrow (1 - \delta)$
$\mathcal{S} \leftarrow$ random subset of $p \cdot \mathcal{I}_{width} \cdot \mathcal{I}_{height}$ pixels in $\mathcal{I}$
$\hat{\mathcal{I}} \leftarrow \mathcal{I}$
foreach pixel *in* $\mathcal{S}$ **do**
    set intensity of pixel to 127 in $\hat{\mathcal{I}}$
end

III. Experiments

A. Methodology

We implement the above four differentially private mechanisms in Python 3 and empirically evaluate their performance on utility and privacy measures. Our experiments were conducted on a Linux machine utilizing a 2.20 GHz processor and 12 GB of RAM.

1) Datasets: We analyze the performance of the mechanisms on two widely used datasets: CASIA-IrisV2 (CASIA) [10] and AT&T Database of Faces (AT&T) [22]. CASIA is a collection of iris images containing 2400 images from 60 subjects, and the images have a resolution of 640×480 pixels. AT&T contains 400 face images from 40 subjects, and each image has a resolution of 92×112 pixels.

2) Default Parameter Values: The privacy parameters, i.e., ϵ and δ, indicate the level of privacy protection. For ϵ-DP methods (DP-Pix, DP-Samp, and DP-SVD), our evaluation focuses on the range of $\epsilon \in [0.1, 0.5, 1, 5, 10]$; and for Snow, we focus on the range of $\delta \in [0.1, 0.33, 0.4, 0.5, 0.6, 0.7, 0.8]$, as smaller δ values offer little to no usefulness. Other algorithm-specific parameters also help balance privacy and utility, such as b of DP-Pix. The default parameter values used are listed in Table I. Note that the default parameter values are adjusted to the higher image resolution of CASIA, for example, a larger block size (b) for pixelization and a larger number of eigenvalues (i) for SVD. Furthermore, a smaller number of clusters (k) is sufficient for DP-Samp on CASIA. Figure 2 visualizes the sampling candidate pixels while varying the number of clusters, k. We see that less data is required to capture the data structure in CASIA compared to for AT&T , e.g. when $k = 8$.

3) Generic Utility Measures: Mean Squared Error (MSE) and Structural Similarity (SSIM) [28] are adopted to quantify the usefulness of the image obfuscation methods. Both measures are computed between the source and the obfuscated images. MSE measures the difference between two images pixel-wise; SSIM captures the differences in the perceived quality (e.g. structure, lighting, contrast) of images. These measures are computed across all images in each dataset and the average value is reported.

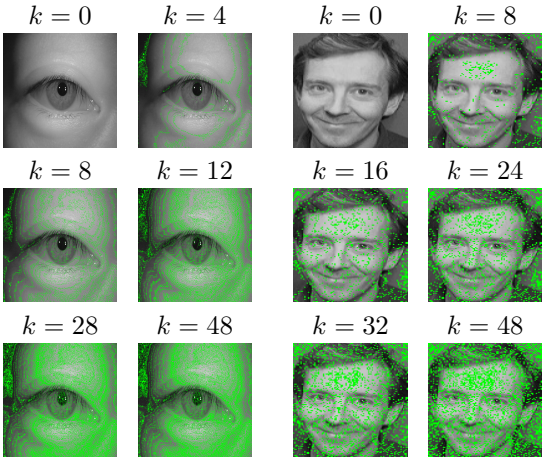

Fig. 2: Pixels as sampling candidates for DP-Samp at varying values of k on CASIA and AT&T datasets

4) Task Based Utility: We adopt *pupil confidence* and *gaze error* as task based utility measures, to support eye-tracking applications [19], [31]. Specifically, for each image in the CASIA dataset, we utilize the DeepVOG [30] framework to compute a pupil confidence score and to estimate the gaze in both the x (yaw) and y (pitch) directions. We report the percentage of images with a confidence score ≥ 0.8, similar to [13]. Furthermore, we compute the gaze error (in $^\circ$) for gaze estimates obtained from the source image and the obfuscated image and report the average across the CASIA dataset.

5) Privacy Risk Measures: In addition to the rigorous differential privacy guarantees, we propose to evaluate the practical privacy protection offered by the existing methods. Since each image can be obfuscated locally, this study focuses on the practical privacy risks associated with sharing the obfuscated images.

Correct Recognition Rate (CRR). For iris images, an important privacy risk is that an obfuscated image of a target individual may be used by an adversary for authentication [3]. For example, the adversary may aim to unlock the target's online account or device, which stores the target's iris baseline (e.g., template), with the obfuscated iris image. To evaluate such risks, we adopt widely used iris segmentation and recognition solutions [8], [16] to extract a binary iris signature for CASIA images. Specifically and similarly to [12], we partition the dataset such that 2 randomly selected images for each individual are set aside as *baselines*, and the rest of images for the individual will be used for recognition. To authenticate an image, Hamming distances are computed between its iris signature and two baseline signatures of the same individual. If the lower distance is below a pre-defined threshold, the authentication is considered successful. In our evaluation, 0.35 is used as the threshold for a successful match, in order to achieve a low false positive rate on real CASIA images. For obfuscated images, we compute the correct recognition rate

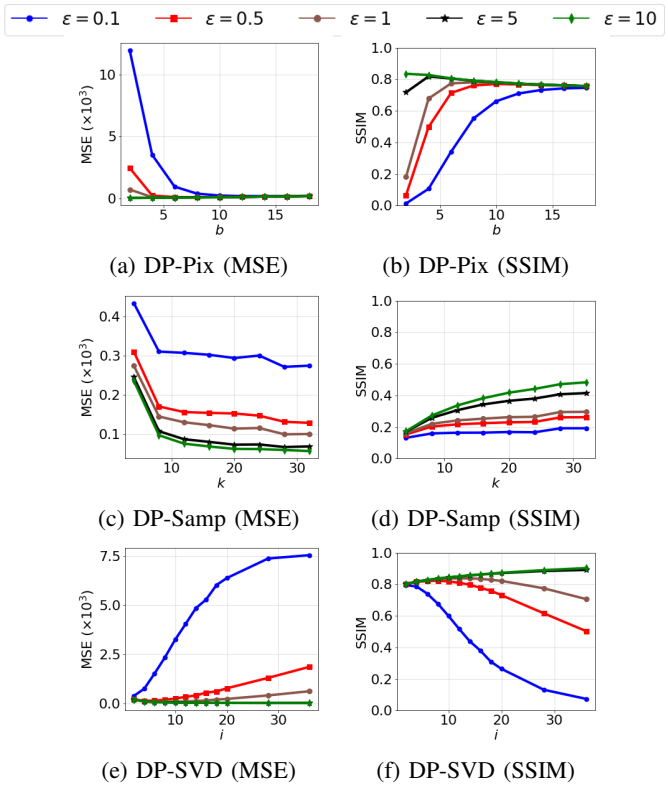

(a) DP-Pix (MSE) (b) DP-Pix (SSIM)

(c) DP-Samp (MSE) (d) DP-Samp (SSIM)

(e) DP-SVD (MSE) (f) DP-SVD (SSIM)

Fig. 3: Mean Squared Error (MSE) and Structural Similarity (SSIM) results of varying algorithm parameters on CASIA dataset

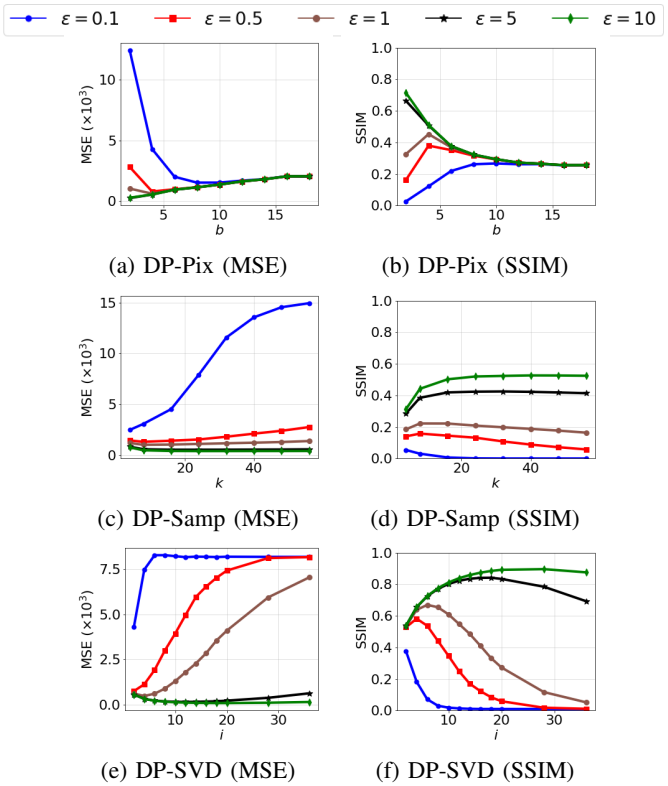

(a) DP-Pix (MSE) (b) DP-Pix (SSIM)

(c) DP-Samp (MSE) (d) DP-Samp (SSIM)

(e) DP-SVD (MSE) (f) DP-SVD (SSIM)

Fig. 4: Mean Squared Error (MSE) and Structural Similarity (SSIM) results of varying algorithm parameters on AT&T dataset

(CRR) as the percentage of obfuscated images successfully matched with their corresponding baselines. Higher values of CRR indicate higher privacy risks.

Face Re-Identification. For face images, a widely adopted privacy measure is the risk of re-identification based on convolutional neural networks (CNN) [6], [18]. In this setting, an adversary has access to some clear face images of all individuals (e.g., from social media); the adversary can apply any obfuscation method to those images and train a CNN model to predict the identity of an obfuscated image. When a new obfuscated image is available (e.g., a pixelized face in a news article), the adversary applies the trained CNN model to infer the identity of the individual. In our evaluation and similar to [6], [18], we partition the AT&T dataset by randomly selecting 8 images for each individual as training and the remaining 2 images for each individual as testing. A CNN model is trained for each obfuscation method and each parameter value. The accuracy on the testing set is reported in our results, with higher values indicating higher privacy risks.

B. Varying Parameters

In this section, we vary the parameters of the studied privacy methods and study their effects on utility. Furthermore, we study those effects under different privacy levels, i.e., by varying ϵ and δ values. The results for CASIA and AT&T are reported in Figure 3 and Figure 4, respectively.

1) Varying b in DP-Pix: First we evaluate the effect of b on the DP-Pix method. Recall that b specifies the block width in pixels used for image pixelization. In Figure 3a and Figure 3b, we observe that for lower epsilon values, MSE first decreases as b increases and begins to increase when b is larger. The "elbow" point is different for each ϵ value. For instance, in Figure 3b, the elbow point is $b = 4$ for $\epsilon = 0.5$ and 1, and $b = 10$ for $\epsilon = 0.1$. For larger epsilon values, there is no observed elbow points. The reason is that increasing b incurs a higher loss of information, i.e., via pixelization, but it helps reduce the magnitude of the Laplace perturbation error introduced by differential privacy, i.e., with scale $\frac{255m}{b^2\epsilon}$. The observed elbow point indicates the b value that minimizes the combined information loss and perturbation error. For sufficiently large ϵ, i.e., small perturbation error, it is always beneficial to adopt a small b value. The results of SSIM (Figure 3b and Figure 4b) are consistent with the MSE results. Note that SSIM is a similar measure, hence the higher the better.

2) Varying k in DP-Samp: For this method, we evaluate the number of pixel intensities selected for sampling. On both datasets, we observe an initial decrease in MSE for smaller values of k (e.g. $k \leq 10$ in Figure 3c and Figure 4c.) As k gets large, we observe from Figure 3c a decrease in MSE on CASIA for low ϵ values ($\epsilon \leq 1$,) and a plateau for all other ϵ values. On AT&T, we observe the increase of k leads to an increase in MSE for smaller ϵ values, e.g., $\epsilon = 0.1$ in Figure 4c. The reason is when sampling is performed according to Equations 2 and 3, the privacy budget is allocated to each intensity. Given a sufficiently small ϵ, the allocated budgets for k intensities may be too small, leading to a higher

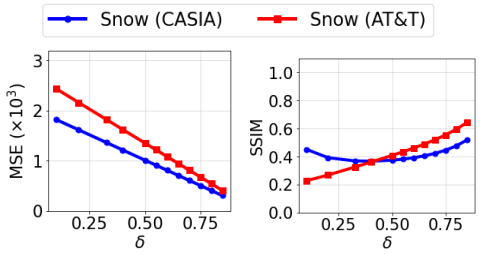

(a) MSE (b) SSIM

Fig. 5: Varying δ parameter of Snow on CASIA and AT&T datasets

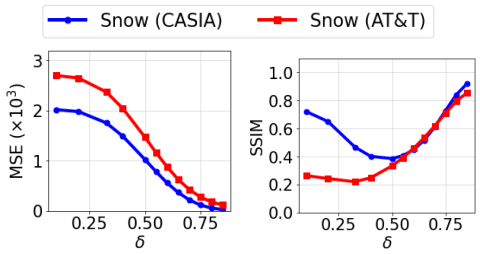

(a) MSE (b) SSIM

Fig. 6: Varying δ parameter of Snow with median blur on CASIA and AT&T datasets

MSE in the obfuscated image. For larger ϵ values, we observe an elbow point in MSE, e.g., $k = 8$ when $\epsilon \geq 0.5$ for AT&T, which indicates a trade-off between more pixel intensities and a smaller privacy budget for each intensity, as k increases. Note that CASIA dataset has a higher resolution and therefore the trade-off is not obvious. The SSIM results for both datasets in Figure 3d and Figure 4d show that DP-Samp does not preserve the structural information in the obfuscated image: the SSIM measure is constantly lower than 0.6, despite increasing the privacy budget ϵ. Moreover, the results show that the structure of AT&T images is more sensitive to changes in k than CASIA images.

3) Varying i in DP-SVD: We investigate the effects of the number of eigenvalues (i) preserved in DP-SVD on utility. Similarly to the other methods, increasing i lead to different effects at different privacy levels. In Figure 3e and Figure 4e, increasing i leads to higher MSE errors in both CASIA and AT&T with small ϵ values (e.g., $\epsilon = 0.1$). For larger ϵ values, e.g., $\epsilon \geq 5$, the MSE first decreases and then increases. The reason is a higher number of eigenvalues allows more information of the original image to be preserved, but would inflict larger perturbation errors by private sampling in higher dimensional spaces. As a result, an elbow point, i.e., lowest total error, is observed when ϵ is sufficiently large; and such ϵ values also depend on the input image, e.g., its resolution and structural complexity. The SSIM results in Figure 4f show the trade-off more clearly. Both Figure 3f and Figure 4f show that higher SSIM scores can be achieved if relaxing privacy; and DP-SVD outperforms DP-Pix and DP-Samp.

4) Varying δ in Snow: Recall Snow satisfies ϵ, δ-DP with $\epsilon = 0$. The method employs a single parameter for pixel sampling, i.e., δ, which also indicates the probability of breaching ϵ-DP. In DP studies, δ is usually set to a small value to ensure adequate privacy protection [5]. For instance, we can set $\delta = \frac{1}{n}$ where n is the number of pixels in the input image, in order to protect each pixel. However, such δ values lead to graying the majority of the image (see Algorithm 4), hence no practical usefulness. In Figure 5, we varying δ between 0.1 and 0.85 to study the utility empirically. For both CASIA and AT&T, increasing δ leads to lower MSE errors (Figure 5a), as fewer pixels are grayed out. In Figure 5b, we observe the SSIM first reduces and then increases for the CASIA dataset. We believe that due to the simple structure of CASIA images, SSIM does not capture the difference between the original image and the obfuscated image when most pixels are grayed out (i.e., smaller δ). We also evaluated an extension of Snow (Figure 6), by applying median blur with a 3×3 kernel to the output image. As can be seen in Figure 6b, the median blur improves the image quality when $\delta > 0/5$, i.e., when the majority of the pixels are preserved. For the CASIA dataset, applying median blur in low δ settings (e.g.,$\delta \leq 0.2$) also leads to higher SSIM scores, due to the limitation of SSIM when the majority of the pixels are grayed out, as discussed previously. We see that face images from AT&T, which have more complex structures, are affected by this lack of robustness to a lesser extent.

Table II: Task Based Utility

	Pupil Confidence			Gaze Error (°)		
ϵ	DP-Pix	DP-Samp	DP-SVD	DP-Pix	DP-Samp	DP-SVD
0.01	47%	0%	30%	5.48	-	56.98
0.05	46%	2%	46%	4.30	10.41	44.39
0.1	47%	6%	47%	4.38	10.92	21.53
0.5	43%	40%	79%	5.79	5.66	2.58
1	45%	56%	77%	5.09	5.09	2.19
5	45%	77%	77%	4.98	3.02	2.08
10	46%	83%	77%	4.50	2.72	2.07

C. Varying m for neighboring images

In the definition of differential privacy, the parameter m determines the number of pixels that may differ between two neighboring images. Larger values of m provide stronger privacy protection, i.e., stronger indistinguishability guarantees, which may require larger perturbation errors. In this evaluation, we adapt DP-Pix and DP-Samp to different m values, while DP-SVD and Snow are not applicable. The utility results are reported for CASIA and AT&T datasets in Figures 7 and 8, respectively. As can be seen, increasing m incurs larger MSE errors and lower SSIM scores for DP-Pix and DP-Samp in both datasets. For CASIA datasets, DP-Samp inflicts lower MSE errors than DP-Pix, enjoying the benefits of pixel sampling in higher resolution images; but in AT&T dataset, DP-Samp does not have the same advantage. The results of SSIM show that DP-Pix outperforms DP-Samp when increasing m and provides high quality consistently in high ϵ settings, thanks to preserving the high-level image structure with pixelization.

D. Practical Utility and Privacy Measures

Next, we discuss task based utility measures and practical privacy risks of the methods at varying privacy levels. Results are reported in Tables II, III, IV, and V. Note that in gaze

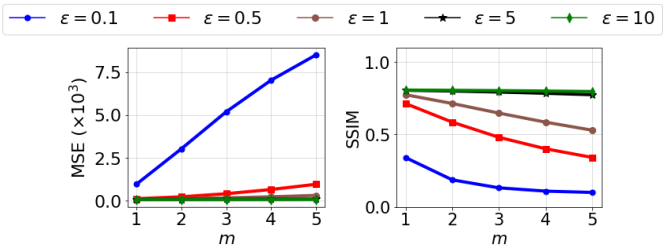

(a) DP-Pix (MSE) (b) DP-Pix (SSIM)

(c) DP-Samp (MSE) (d) DP-Samp (SSIM)

Fig. 7: Results of varying m on CASIA dataset

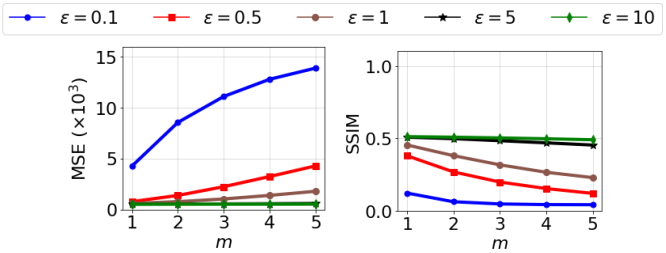

(a) DP-Pix (MSE) (b) DP-Pix (SSIM)

(c) DP-Samp (MSE) (d) DP-Samp (SSIM)

Fig. 8: Results of varying m on AT&T dataset

Table III: Privacy Risk Measures

	CRR - CASIA			Re-ID - AT&T		
ϵ	DP-Pix	DP-Samp	DP-SVD	DP-Pix	DP-Samp	DP-SVD
0.01	0%	0%	0%	3%	0%	1%
0.05	0%	0%	0%	9%	3%	3%
0.1	0%	0%	0%	10%	11%	58%
0.5	0%	0%	0%	68%	35%	63%
1	0%	0%	0%	68%	51%	56%
5	0%	4%	0%	83%	77%	59%
10	0%	7%	0%	81%	83%	60%

Table IV: Task Based Utility - Snow

	Pupil Confidence		Gaze Error (°)	
δ	Snow	Snow-Med	Snow	Snow-Med
0.1	0%	0%	-	-
0.33	30%	0%	3.20	-
0.4	64%	2%	2.17	6.58
0.5	80%	50%	1.76	3.06
0.6	87%	82%	1.42	1.86
0.7	92%	94%	0.95	0.88
0.8	94%	99%	0.58	0.28

Table V: Privacy Risk Measures - Snow

	CRR - CASIA		Re-ID - AT&T	
δ	Snow	Snow-Med	Snow	Snow-Med
0.1	0%	0%	4%	4%
0.33	0%	0%	13%	5%
0.4	0%	0%	23%	4%
0.5	0%	0%	75%	9%
0.6	1%	0%	86%	54%
0.7	5%	25%	85%	81%
0.8	10%	77%	91%	91%

error results, a dash (-) is used to indicate that the gaze error could not be determined due to a 0% pupil detection rate.

1) Task Based Utility: In Table II, we observe that when the privacy protection in stronger ($\epsilon \leq 0.1$), DP-Pix provides higher pupil confidence scores and lower gaze errors, compared to DP-Samp and DP-SVD; however, those utility measures do not improve when increasing ϵ, due to the information loss incurred by pixelization. Increasing ϵ for DP-Samp and DP-SVD leads to higher pupil confidence and lower gaze errors. We observe that DP-SVD quickly achieves high utility at a low privacy cost, e.g., $\epsilon = 0.5$. In Table IV, it can be seen that increasing δ values in Snow improves pupil confidence and gaze error, with or without median blur. Note that with median blur, Snow achieves better utility in both measures at low privacy settings, i.e., $\delta \geq 0.7$, as the median blur removes noise effectively when sufficient pixels are sampled from the input image.

2) Privacy Risks: We observe in Table III that both DP-Pix, DP-Samp, and DP-SVD are shown to be resistant to iris authentication based attacks at all privacy levels, i.e., 0% CRR, while DP-Samp allows a small percentage of matches at high ϵ settings. It shows that the privacy perturbation inflicted by DP-Pix and DP-SVD successfully prevents the obfuscated image to be matched to existing templates. As DP-Samp outputs pixels from the real image, some obfuscated images may be matched at high ϵ settings. As seen in Table V, Snow leads to at most 10% CRR; however, applying median blur leads to up to 77% CRR at high δ settings. Since median blur can be applied by any adversary on the output image, we conclude that Snow does not provide strong defense against iris authentication attacks.

The face re-identification attack shows whether deep learning models can *adapt* to the evaluated obfuscation methods. It can be seen in Table III that DP-Pix and DP-Samp lead to up to 83% re-identification rates at high ϵ settings, while DP-SVD inflicts lower risks despite the increase in ϵ. In Table V, we observe that Snow and Snow-Med lead to high re-identification risks, up to 91%. Even in lower δ settings (e.g., $\delta \leq 0.5$), Snow inflicts up to 75% re-identification risks due to the disclosure of real pixels.

3) CPU Time: We measure the runtime for each obfuscation method to sanitize a single image and the results are reported in Figure 9. In general, higher runtimes can be observed on the CASIA dataset for every method, due to a higher resolution. Across all methods, the privacy level (ϵ or δ) does not affect the runtime performance of the obfuscation. DP-Samp inflicts the highest runtimes among all methods,

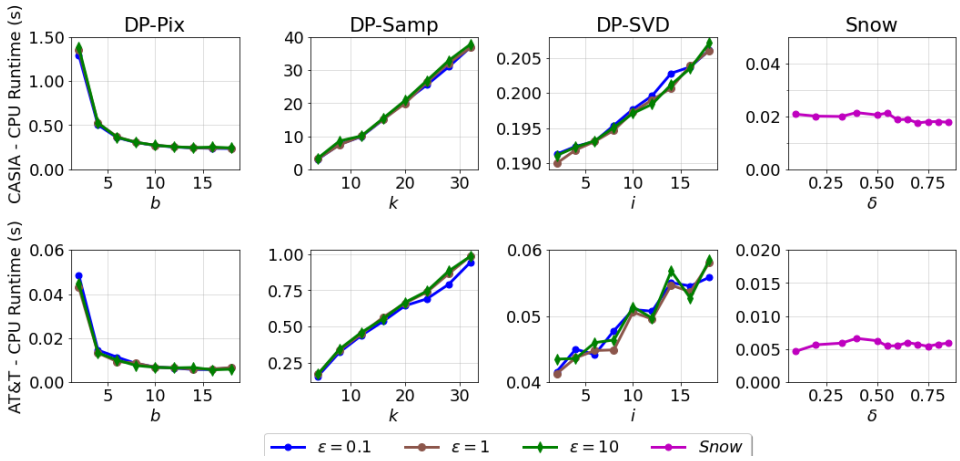

Fig. 9: Runtimes of DP-Pix, DP-Samp, DP-SVD, and Snow for sanitizing one image.

due to the computational costs inflicted by pixel clustering and sampling; a higher number of clusters (k) leads to higher runtimes. For DP-Pix, increasing the block width b reduces the runtime as perturbation is performed on a smaller number of blocks. For DP-SVD, increasing the number of eigenvalues i increases the runtime as the method conducts private sampling in a higher dimensional space.

E. Qualitative Evaluation

We also provide sample output images (Figure 10) produced by the obfuscation methods with different parameter values and privacy levels, to enable a qualitative evaluation. For CASIA dataset, DP-Samp introduces higher distortions to the eyes with $\epsilon = 0.5$, compared to other methods. DP-SVD does not capture detailed features, e.g., eyebrows, while DP-Pix and Snow introduce "salt and pepper" noise. Increasing ϵ to 1 reduces the distortions and perturbations in DP-Samp and DP-SVD, and improves the output quality of DP-Pix greatly. Applying median blur to Snow may aggravate the gray noise at low δ settings and help remove such noise at high δ settings.

For AT&T dataset, DP-Samp produces low quality output images among all methods. DP-SVD introduces distortions due to matrix singular value decomposition and private sampling, but distortions incurred by sampling are alleviated effectively by increasing ϵ to 1. DP-Pix outputs show the effects of pixelization and privacy perturbation, and the perturbation effect may be reduced by adopting a higher b value and/or a higher ϵ value. Due to a lower resolution, the outputs of Snow and Snow-Med are affected by the gray noise much more than for CASIA.

IV. Discussion

A. Interpreting the results

We have made several observations which may provide insights for adopting existing obfuscation methods and developing new image obfuscation methods.

Firstly, although lower pixel-level errors, i.e., MSE, often lead to higher SSIM scores, it does not always hold for images with simple structures, e.g., CASIA eye images. Our results in Figure 3c showed that DP-Samp inflicts MSE errors equal to or smaller than those of DP-Pix (Figure 3a) and DP-SVD (Figure 3e), while its SSIM scores are lower in most instances. For Snow, the MSE errors for CASIA dataset monotonically decrease when increasing δ (see Figures 5a and 6a), while the SSIM scores (see Figures 5b and 6b) at $\delta = 0.1$ are much higher than that of other δ values. The sample output images in Figure 10 show that the SSIM measure alone may not be sufficient to capture the quality for images with simple structures.

Secondly, we observe that low generic utility (MSE and SSIM) does not always lead to low task-based utility. For example, DP-Pix in low ϵ settings (e.g., $\epsilon \leq 0.1$) leads to high MSE errors and low SSIM scores, shown in Figures 3a and 3b; it provides higher pupil confidence (46%) and lower gaze errors ($5.48°$) than other methods when $\epsilon \leq 0.1$, shown in Table II. It shows that pixelization-based obfuscation can provide some usefulness for image applications, even at low ϵ settings.

Thirdly, we observe that the obfuscation methods exhibit distinct trade-off behaviors between privacy and task-based utility. As seen in Tables II and IV, DP-Pix provides stable pupil confidence and gaze errors when increasing ϵ; DP-Samp and DP-SVD show rapid improvements in those measures between $\epsilon = 0.1$ and $\epsilon = 0.5$; Snow gradually improves as δ increases. We believe that the design of the method plays an important role: DP-Pix employs pixelization, which inflicts a loss of detailed information independent of the differential privacy guarantees. DP-Samp and DP-SVD utilize the global structure/features in the input image, which may not be accurately captured at low ϵ settings. Snow outputs each pixel independently, which results in the gradual utility improvement by increasing the sampling probability.

Last but not least, we observe that although theoretical privacy guarantees often correlate with practical privacy protection, post-processing may change the level of practical privacy protection. In Table III, we see that the practical privacy risks increase when ϵ increases for DP-Pix, DP-Samp, and DP-SVD. In Table V, we see that applying median blur after Snow significantly increases the CRR, e.g., from 10% to 77% for $\delta = 0.8$, although median blur does not weaken the

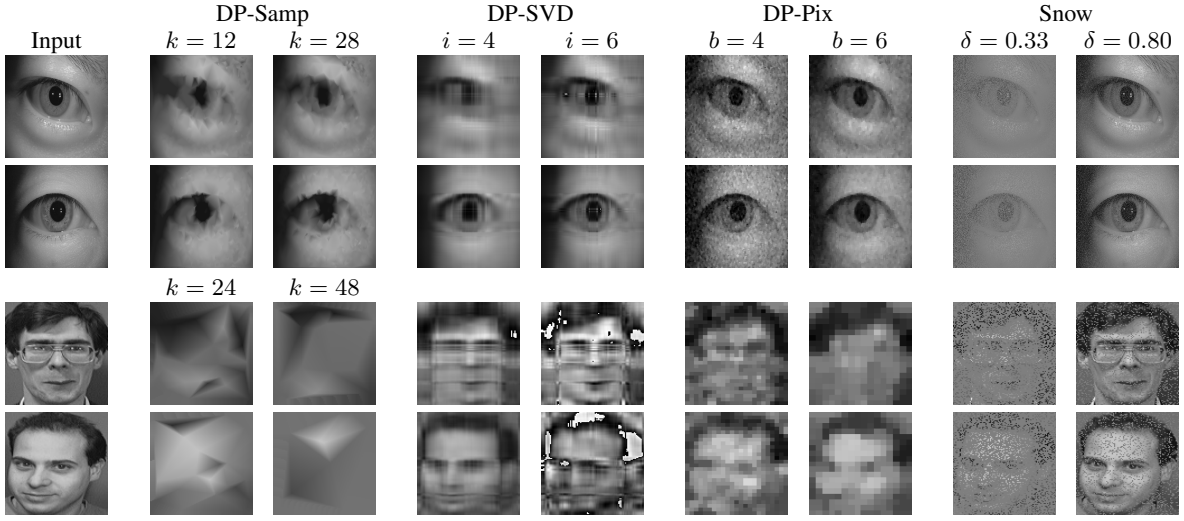

(a) $\epsilon = 0.5$ for DP-Pix, DP-Samp, and DP-SVD. Snow is not affected by ϵ.

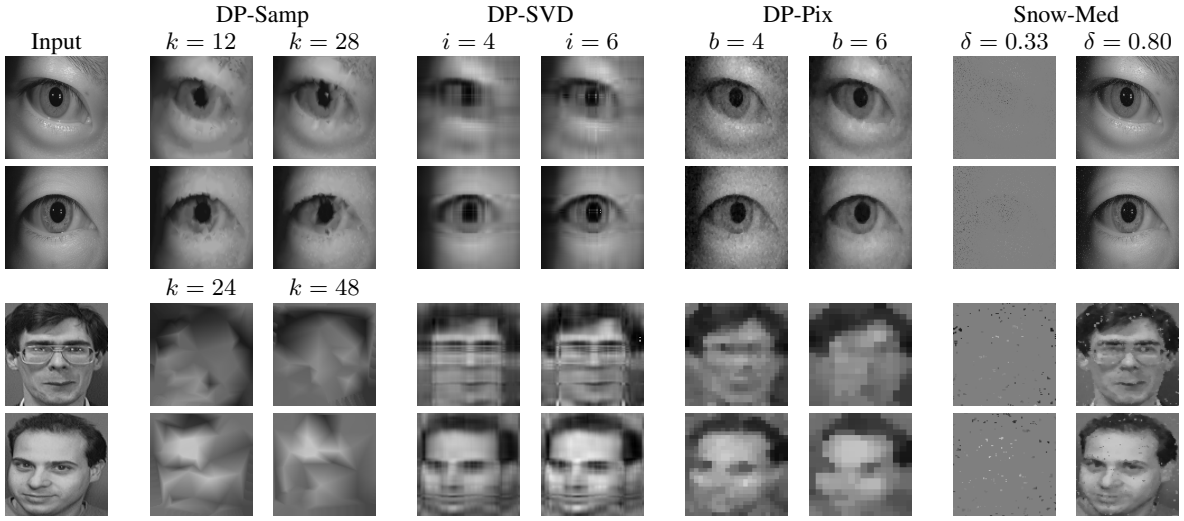

(b) $\epsilon = 1$ for DP-Pix, DP-Samp, and DP-SVD. Snow-Med is not affected by ϵ.

Fig. 10: Sample output images produced by DP-Samp, DP-SVD, and DP-Pix at $\epsilon = 0.5$ and 1, as well as by Snow and Snow-Med (i.e., with median blur) at $\delta = 0.33$ and 0.80.

differential privacy guarantees.

B. How to choose

There is no "one size fits all" solution. It is important to recognize that applications may have different priorities and requirements for image obfuscation. For applications requiring provable privacy guarantees, DP-Pix provides ϵ-DP guarantees and can be adapted to protecting more than one pixels in the input image. Both DP-SVD and Snow provide relaxed DP guarantees, i.e., metric privacy and (ϵ, δ)-DP, respectively. DP-Samp provides ϵ-DP for individual pixels on some steps but not in the pixel grouping step. For applications requiring strong practical privacy protection, DP-Pix with $\epsilon \leq 0.1$ is a great option, thanks to low privacy risks in Table III and much better utility measures compared to other methods in Table II. For applications wishing for a balance between privacy and utility, DP-SVD or DP-Samp with $\epsilon = 0.5$ may be considered: as shown in Table II, DP-SVD provides 79% pupil confidence and 2.58° gaze error, while DP-Samp provides 40% pupil confidence and 5.66° gaze error; but DP-SVD leads to a higher Re-ID risk than DP-Samp in Table III, i.e., 63% vs 35%. With even weaker privacy guarantees, applications may consider Snow with $\delta = 0.5$, which achieves 80% pupil confidence, 1.76° gaze error, and 75% Re-ID risk (see Tables IV and V). Additional considerations such as computational resources and runtime requirements should also be taken to account.

C. Extension to Multi-Channel Images.

Considering image data with multiple channels, such as RGB (red-green-blue) and HSV (hue-saturation-value) images, each channel may not be independent of the other channels. A straight-forward extension of image DP is to split the privacy budget, i.e., ϵ and δ, across multiple channels and apply DP methods accordingly.

V. Conclusion

In this work we performed a comprehensive evaluation of four image obfuscation methods, namely DP-Pix, DP-

Samp, DP-SVD, and Snow, that provide differential privacy guarantees. We adopted real eye and face image datasets and evaluated both generic and task based utility measures as well as practical protection against privacy attacks. Our results show that the application domain is an important factor in evaluating image obfuscation methods. For instance, with the CASIA dataset, Snow with median blur achieves a high SSIM score at $\delta = 0.1$ but inflicts a large MSE error and very low task-based utility. We found that DP-Pix provides pure ϵ-DP; it achieves the best task-based utility in strong privacy settings (i.e., $\epsilon \leq 0.1$) with low empirical privacy risks. For moderate to low privacy settings (i.e., $\epsilon \geq 0.5$), DP-SVD and DP-Samp provide a trade-off between privacy and utility, while DP-SVD achieves lower gaze errors and lower privacy risks even in low privacy settings (e.g., $\epsilon = 10$). Snow provides (ϵ, δ)-DP and may achieve higher task-based utility at the cost of high practical privacy risks, e.g., 77% CRR for eye images.

For future work, the following directions may be considered. 1) The development of new image obfuscation methods for specific domain applications: Snow and DP-SVD adopt different approaches to serve the target domains (i.e., eye-tracking applications and face images, respectively). Future work should take into account of the characteristics of the data and applications, in order to achieve high usefulness. 2) The development of new privacy risk measures: this study focused on *identity* based privacy attacks due to its sensitivity, while the disclosure of other information may also be considered, such as emotion, activity, etc. 3) The development of new obfuscation methods to produce more natural looking images: current methods may produce visually unappealing images, e.g., DP-Pix, thus unlikely adopted in the popular media. Future research may leverage latest machine learning techniques to generate natural looking images, while providing rigorous privacy guarantees.

REFERENCES

[1] M. E. Andrés, N. E. Bordenabe, K. Chatzikokolakis, and C. Palamidessi. Geo-indistinguishability: Differential privacy for location-based systems. In *Proceedings of the 2013 ACM SIGSAC Conference on Computer & Communications Security*, CCS '13, page 901–914, New York, NY, USA, 2013. Association for Computing Machinery.

[2] K. Chatzikokolakis, M. E. Andrés, N. E. Bordenabe, and C. Palamidessi. Broadening the scope of differential privacy using metrics. In E. De Cristofaro and M. Wright, editors, *Privacy Enhancing Technologies*, pages 82–102, Berlin, Heidelberg, 2013. Springer Berlin Heidelberg.

[3] J. Daugman. How iris recognition works. In *The essential guide to image processing*, pages 715–739. Elsevier, 2009.

[4] C. Dwork, F. McSherry, K. Nissim, and A. Smith. Calibrating noise to sensitivity in private data analysis. In S. Halevi and T. Rabin, editors, *Theory of Cryptography*, pages 265–284, Berlin, Heidelberg, 2006. Springer Berlin Heidelberg.

[5] C. Dwork and A. Roth. The algorithmic foundations of differential privacy. *Found. Trends Theor. Comput. Sci.*, 9(3–4):211–407, Aug. 2014.

[6] L. Fan. Image pixelization with differential privacy. In F. Kerschbaum and S. Paraboschi, editors, *Data and Applications Security and Privacy XXXII*, pages 148–162, Cham, 2018. Springer International Publishing.

[7] L. Fan. Practical image obfuscation with provable privacy. *2019 IEEE International Conference on Multimedia and Expo (ICME)*, pages 784–789, 2019.

[8] A. Gangwar, A. Joshi, A. Singh, F. Alonso-Fernandez, and J. Bigun. Irisseg: A fast and robust iris segmentation framework for non-ideal iris images. In *2016 International Conference on Biometrics (ICB)*, pages 1–8, 2016.

[9] M. Guevara. How we're helping developers with differential privacy [last accessed 08-04-2021]. developers.googleblog.com/2021/01/how-were-helping-developers-with-differential-privacy.html, Jan 2021.

[10] Z. He, T. Tan, Z. Sun, and X. Qiu. Toward accurate and fast iris segmentation for iris biometrics. *IEEE Transactions on Pattern Analysis and Machine Intelligence*, 31(9):1670–1684, 2009.

[11] S. Hill, Z. Zhou, L. Saul, and H. Shacham. On the (in)effectiveness of mosaicing and blurring as tools for document redaction. *Proceedings on Privacy Enhancing Technologies*, 2016, 02 2016.

[12] B. John, S. Jörg, S. Koppal, and E. Jain. The security-utility trade-off for iris authentication and eye animation for social virtual avatars. *IEEE Transactions on Visualization and Computer Graphics*, 26:1880–1890, 2020.

[13] B. John, A. Liu, L. Xia, S. Koppal, and E. Jain. Let it snow: Adding pixel noise to protect the user's identity. In *ACM Symposium on Eye Tracking Research and Applications*, ETRA '20 Adjunct, New York, NY, USA, 2020. Association for Computing Machinery.

[14] V. V. John Abowd. Modernizing privacy protections for the 2020 census: Next steps [last accessed 08-04-2021]. www.census.gov/newsroom/blogs/random-samplings/2021/04/modernizing_privacy.html, April 2021.

[15] S. Kamijo, Y. Matsushita, K. Ikeuchi, and M. Sakauchi. Traffic monitoring and accident detection at intersections. *IEEE Transactions on Intelligent Transportation Systems*, 1(2):108–118, 2000.

[16] L. Masek. *Recognition of Human Iris Patterns for Biometric Identification*. PhD thesis, The University of Western Australia, 2003.

[17] R. McPherson, R. Shokri, and V. Shmatikov. Defeating image obfuscation with deep learning. *CoRR*, abs/1609.00408, 2016.

[18] R. McPherson, R. Shokri, and V. Shmatikov. Defeating image obfuscation with deep learning. *CoRR*, abs/1609.00408, 2016.

[19] S. Park, X. Zhang, A. Bulling, and O. Hilliges. Learning to find eye region landmarks for remote gaze estimation in unconstrained settings. ETRA '18, New York, NY, USA, 2018. Association for Computing Machinery.

[20] A. Reece and C. Danforth. Erratum to: Instagram photos reveal predictive markers of depression. *EPJ Data Science*, 6, 12 2017.

[21] Z. Ren, Y. J. Lee, and M. S. Ryoo. Learning to anonymize faces for privacy preserving action detection. *CoRR*, abs/1803.11556, 2018.

[22] F. Samaria and A. Harter. Parameterisation of a stochastic model for human face identification. In *Proceedings of 1994 IEEE Workshop on Applications of Computer Vision*, pages 138–142, 1994.

[23] R. Stevens and I. Pudney. Blur select faces with the updated blur faces tool, 12 2012.

[24] D. Su, J. Cao, N. Li, E. Bertino, M. Lyu, and H. Jin. Differentially private k-means clustering and a hybrid approach to private optimization. *ACM Transactions on Privacy and Security (TOPS)*, 20(4):1–33, 2017.

[25] Q. Sun, L. Ma, S. J. Oh, L. Van Gool, B. Schiele, and M. Fritz. Natural and effective obfuscation by head inpainting. pages 5050–5059, 06 2018.

[26] A. D. P. Team. Learning with privacy at scale [last accessed 08-04-2021]. machinelearning.apple.com/research/learning-with-privacy-at-scale, Dec 2017.

[27] H. Wang, S. Xie, and Y. Hong. Videodp: A flexible platform for video analytics with differential privacy. *Proc. Priv. Enhancing Technol.*, 2020(4):277–296, 2020.

[28] Z. Wang, A. Bovik, H. Sheikh, and E. Simoncelli. Image quality assessment: from error visibility to structural similarity. *IEEE Transactions on Image Processing*, 13(4):600–612, 2004.

[29] Y. Yang, J. Liu, and M. Shah. Video scene understanding using multi-scale analysis. In *2009 IEEE 12th International Conference on Computer Vision*, pages 1669–1676. IEEE, 2009.

[30] Y.-H. Yiu, M. Aboulatta, T. Raiser, L. Ophey, V. L. Flanagin, P. zu Eulenburg, and S.-A. Ahmadi. Deepvog: Open-source pupil segmentation and gaze estimation in neuroscience using deep learning. *Journal of neuroscience methods*, 2019.

[31] X. Zhang, Y. Sugano, M. Fritz, and A. Bulling. Appearance-based gaze estimation in the wild. In *Proceedings of the IEEE conference on computer vision and pattern recognition*, pages 4511–4520, 2015.